Ligand-field Symmetry Effects in Fe(II) Polypyridyl Compounds Probed by Transient X-ray Absorption Spectroscopy

Hana Cho,[ab] Matthew L. Strader,[a] Kiryong Hong,[b] Lindsey Jamula,[c] Tae Kyu Kim, [*b] Frank M. F. de Groot,[d] James K. McCusker,[c] Robert W. Schoenlein,[a] and Nils Huse[*ae]

[a] *Ultrafast X-ray Science Laboratory, Chemical Sciences Division, Lawrence Berkeley National Laboratory, Berkeley, California, USA.*
[b] *Department of Chemistry and Chemistry Institute of Functional Materials, Pusan National University, Busan, Republic of Korea. E-mail: tkkim@pusan.ac.kr*
[c] *Department of Chemistry, Michigan State University, East Lansing, Michigan, USA.*
[d] *Department of Chemistry, Utrecht University, Utrecht, Netherlands.*
[e] *Max Planck Research Department for Structural Dynamics at the University of Hamburg & Center for Free Electron Laser Science, Hamburg, Germany. E-mail: nils.huse@mpsd.cfel.de*

Abstract:

Ultrafast excited-state evolution in polypyridyl Fe^{II} complexes are of fundamental interest for understanding the origins of the sub-ps spin-state changes that occur upon photoexcitation of this class of compounds as well as for the potential impact such ultrafast dynamics have on incorporation of these compounds in solar energy conversion schemes or switchable optical storage technologies. We have demonstrated that ground-state and, more importantly, ultrafast time-resolved x-ray absorption methods can offer unique insights into the interplay between electronic and geometric structure that underpin the photo-induced dynamics of this class of compounds. The present contribution examines in greater detail how the symmetry of the ligand field surrounding the metal ion can be probed using these x-ray techniques. In particular, we show that steady-state K-edge spectroscopy of the nearest-neighbour nitrogen atoms reveals the characteristic chemical environment of the respective ligands and suggests an interesting target for future charge-transfer femtosecond and attosecond spectroscopy in the x-ray water window.

Introduction

Transition metal-based polypyridyl complexes represent a large and important class of inorganic compounds. Historically, compounds of Ru(II), Os(II), and Re(I) have garnered most of the attention from researchers. However, potential limitations of such systems in more applied contexts due to their intrinsic scarcity has refocused attention on complexes based on the more earth-abundant elements of the first transition series; of these, Fe(II)-based chromophores are among the most widely studied in terms of their photophysical properties. In particular, polypyridyl Fe^{II} complexes are considered as potential candidates for dye-sensitizer solar cells.[1,2] Initially, photo-perturbation and laser temperature jump measurements on polypyridyl Fe^{II} spin-crossover (SCO) complexes with a low-spin (LS) $^1A_1$ ground state were used to characterize the transient high-spin (HS) $^5T_2$ state and to determine the intermolecular kinetics of ground-state recovery, i.e., the $^5T_2 \rightarrow {}^1A_1$ relaxation process.[3,4] This HS→LS relaxation can generally be described by a non-adiabatic multi-phonon process in the strong coupling limit that is thermally activated at room-temperature.[5] Freezing out of vibrational excitations results in light-induced excited spin-state trapping (LIESST)[6-8] with tunnelling rates as low as 10^{-6} s^{-1} for high-spin relaxation from the $^5T_2$ ground vibrational state due.[9]

Ultrafast electronic absorption measurements revealed the sub-picosecond dynamics associated with formation of the $^5T_2$ state following photo-excitation of low-spin Fe(II) complexes[10,11] as well as a sub-100 fs time scale of charge transfer-to-ligand field-state conversion.[2] A definitive combined electronic/resonance Raman study detailed a ca. 200 fs time scale for establishment of the $^5T_2$ transient electronic state.[12] Ultrafast optical studies by Chergui and co-workers provided important additional mechanistic information on the ultrafast spin-state conversion with evidence for ultrafast ^{1}MLCT→^{3}MLCT before subsequent population of the $^5T_2$ high-spin state.[13] A detailed theoretical description of these dynamics has yet to be reported, however, a recent study suggested that direct MLCT→$^5T_2$ relaxation may occur due to favourable potential energy surface crossings and the specific charge-transfer character of the $^5T_2$ state.[14] A transient infrared spectroscopic study has reported formations times of the $^5T_2$ state and subsequent intramolecular energy redistribution consistent with the optical studies.[15] Interestingly, no signatures of vibrational coherence of the symmetric breathing mode have been observed, although this mode is likely coupled to the LS→HS conversion due to the ca. 0.2 Å increase in bond length that characterizes the transition. Indeed, the fast population of the $^5T_2$ high-spin state appears to be impulsive on the time-scale of vibrational modes of the $^5T_2$ state, having been assigned as the

origin of vibrational coherences observed upon formation of the transient high-spin state.[16]

Complementary to optical techniques, core-level spectroscopies have provided information on the structural dynamics and the accompany changes in valence charge distribution underlying the SCO transition.[17-23] Compared to time-resolved optical spectroscopy, ultrafast x-ray spectroscopy is chemically very specific due to the highly localized initial state of the core-level transition. Well-separated transition energies allow for probing specific atomic species with information on molecular structures and valence electronic configurations in the excited state.[24-28] Transient extended x-ray absorption fine structure (EXAFS) spectroscopy has been employed to study the structural changes around the metal centre via the Fe K-edge of $[Fe(tren(py)_3)]^{2+}$ and $[Fe(bpy)_3]^{2+}$, providing information on the structural changes (e.g., ~0.2 Å dilation of the Fe–N bonds) subsequent to optical excitation.[17,18] Transient x-ray diffraction from solid-state SCO complexes has revealed a thermal SCO transition following the initial photo-induced SCO and thermalization of the optical excitation.[29] Transient x-ray absorption and emission spectroscopy of first-row transition metals can report on spin-state changes on ultrafast time-scales and can reveal electronic changes associated with valence orbitals of specific symmetry.[21-23] For instance, we have recently demonstrated picosecond and femtosecond XAS in the soft x-ray range of solvated $[Fe(tren(py)_3)]^{2+}$, which provided a detailed picture of the changes in valence electron distributions in the 3*d* manifold of the transient high-spin state in an Fe^{II} complex subsequent to charge-transfer excitation.[21,23] These results underscore the potential of ultrafast L-edge spectroscopy for the study of transition metal chemistry in solution. Furthermore, recent advances in *ab initio* modelling of x-ray absorption near-edge structures (XANES)[30] show very good agreement with experimental at Fe K-edge spectra, allowing for a more detailed and confident interpretation of XANES spectra in general.

In this work, we aim to understand changes of valence charge density in polypyridyl Fe^{II} complexes upon spin-crossover for different, but related, coordination environments of the metal centre. Specifically, we studied the three compounds displayed in Fig. 1 to examine the extent to which steady-state and time-resolved x-ray absorption spectroscopies could provide information concerning small variations in the local ligand field of Fe^{II} ion. The compounds in Fig. 1 are often approximated as possessing O_h symmetry; in reality, the three pyridine and three imine nitrogen donors of compound **1** effectively reduce this to C_3 symmetry. And while compounds **2** and **3** all present pyridine nitrogen donors to the metal centre, distortions due to the geometric constraints of the ligands result in symmetry reductions to C_2 and D_3 symmetry, respectively. In principle, even a slight reduction of molecular symmetry formally lifts some of the orbital degeneracies, which may in turn noticeably affect electronic interactions between the metal centre and the ligands and give rise to detectable perturbations in the x-ray absorption properties of both the ground- and photo-induced excited states of these compounds.

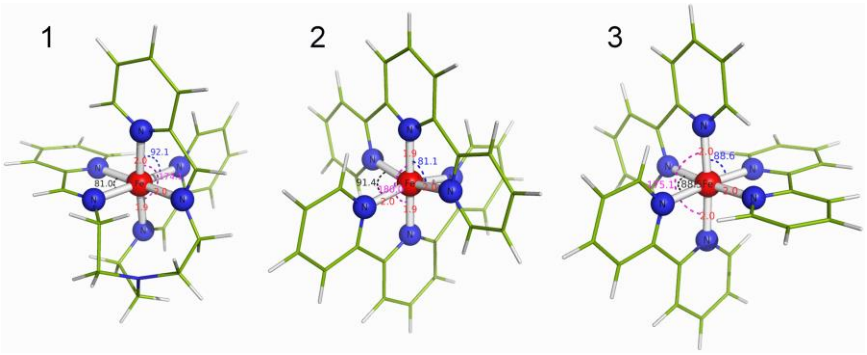

Fig. 1 DFT-derived molecular structures of the investigated polypyridyl Fe^{II} compounds. **1**: $[Fe(tren(py)_3)]^{2+}$. **2**: $[Fe(terpy)_2]^{2+}$. **3**: $[Fe(bpy)_3]^{2+}$. All three compounds feature a pseudo-octahedral arrangement of six nitrogen atoms around the central Fe^{II} ion. The deviations from octahedral symmetry vary but are substantial in all three compounds

Methods

Synthesis. All three of these Fe(II) complexes have been previously reported in the literature. $[Fe(tren(py)_3)](PF_6)_2$ was prepared from $FeCl_2.4H_2O$ reacting with the condensate of three equivalents of 2-pyridine-carboxaldehyde and tris(2-aminoethyl)amine in MeOH solution under a nitrogen atmosphere as described elsewhere.[2] Both $[Fe(terpy)_2](PF_6)_2$ and $[Fe(bpy)_3](PF_6)_2$ were prepared in a similar fashion using $FeCl_2.4H_2O$ and appropriate stoichiometric equivalents of 2,2':6':2"-terpyridine and 2,2'-bipyridine, respectively. The identities and purities of all three samples were confirmed using elemental analysis,

electrospray mass spectroscopy, and comparison of their optical and electrochemical properties with known samples.

Spectral measurements. Solution-phase x-ray absorption spectra of the ground state and transient excited state of the samples were measured at the ultrafast soft x-ray beamline of the Advanced Light Source (ALS) while the ground-state spectra of the crystalline compounds were recorded at the EUV calibration beamline of the ALS. Fig. 2 depicts the general layout of the time-resolved experiment: The ALS synchrotron has a filling pattern with one electron bunch separated from all other bunches by 50 ns gaps. The 70-ps x-ray pulses generated in the beamline undulator by this so-called cam-shaft bunch are recorded by gated detection. A pulsed Ti:Sapphire laser oscillator with 62.5 MHz repetition rate is synchronized to the 500-MHz radio frequency (RF) with which the electron bunches are driven inside the synchrotron. Appropriately selected and amplified 800-nm pulses are converted to 400-nm pulses via second harmonic generation (SHG) and overlapped with the X-rays in the plane of the sample.

Experimental setup. The details of the sample cell and the experimental chamber have been described elsewhere.[21] Briefly, a 2 μm-thick liquid film of a 100 mM acetonitrile solution of polypyridyl Fe^{II} complexes was held between two 100 nm-thick silicon nitride membranes and the solid samples were deposited on a thin silicon nitride substrate with a sample thickness of few hundred nanometres. The liquid samples were excited by 400-nm laser pulses with 3 μJ pulse energy at a repetition rate of 1 kHz and probed with tuneable x-ray pulses at the iron $L_{2,3}$-edges at around 700 eV by recording changes in the transmitted x-ray intensity at 2 kHz (Fig. 2). Transient differential x-ray absorption spectra at fixed time delay and transients at fixed x-ray photon energy were obtained by taking the ratio of x-ray transmitted intensities of the unexcited and laser-excited samples.[27]

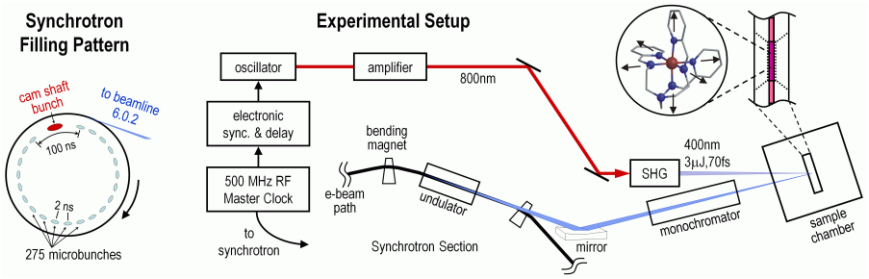

Fig. 2 Schematic of the laser-pump/x-ray-probe experiments at the ultrafast x-ray facility of the Advanced Light Source. The tuneable x-ray pulses produced by the isolated cam shaft electron bunch are focused onto the sample with an imaging monochromator to probe sample transmission changes after laser excitation. The sample is held in a 2 μm thin liquid cell inside a soft x-ray compatible experimental chamber.

Density functional calculations. The LS and HS of ($[Fe(bpy)_3]^{2+}$, $[Fe(terpy)_2]^{2+}$, and $[Fe(tren(py)_3)]^{2+}$) in the gas phase were calculated using density functional theory (DFT). All geometries of these complexes were fully optimized using the hybrid functional of Perdew, Burke, and Ernzerhof (PBE0). We used the effective core potential (ECP) to treat the scalar relativistic effect for Fe. The Los Alamos effective core potential with corresponding valence basis set and polarization *f* functions, LANL08(f) and 6-31G(d,p) basis sets were used for Fe and the other atoms (C, H, and N), respectively. To obtain the zero point energy (ZPE), we carried out vibrational frequency calculations by using the same level of theory. We used the natural population analysis (NPA) for characterization of atomic charges and electronic structures. We also performed the same level of calculations (PBE0/LANL08(f)+6-31G(d,p)) for three Fe^{II} complexes in acetonitrile solution. The solvent calculations used the integral equation formalism variant of the polarizable continuum model (IEFPCM). The program Gaussian 09 was used for all DFT calculations.

Results and Discussion

We have studied the ground and meta-stable excited state via the L-edge spectra of the metal centre upon excitation of the lowest energy metal-to-ligand charge-transfer (MLCT) band (Fig. 3A) by time-resolved x-ray absorption spectroscopy. The probing scheme is illustrated in Fig. 3B where electrons are excited from spin-orbit-split Fe-*2p* core-levels to the unoccupied Fe-*3d* charge density of states. Promoting the highly metal-localized Fe-*2p* core-electrons into the unoccupied valence charge density allows for a metal-centred view of the metal-ligand interactions. This type of core-level spectroscopy can be exploited to extract information on changes of energy levels, valence charge delocalization and bonding, and spin-state changes during the photo-

induced intersystem crossing. In particular, the absorption features at the Fe $L_{2,3}$-edges, arising from dipole-allowed resonant Fe=*2p* transitions, are sensitive to the local electronic structure and dynamic changes in ligand field split Fe-*3d* levels. In the following, we present spectra of metal (Fe L-edges) and ligand (N K-edge) x-ray absorption spectra, and deduce consequences of structural variation of the ligand cage for the valence charge density of transient states.

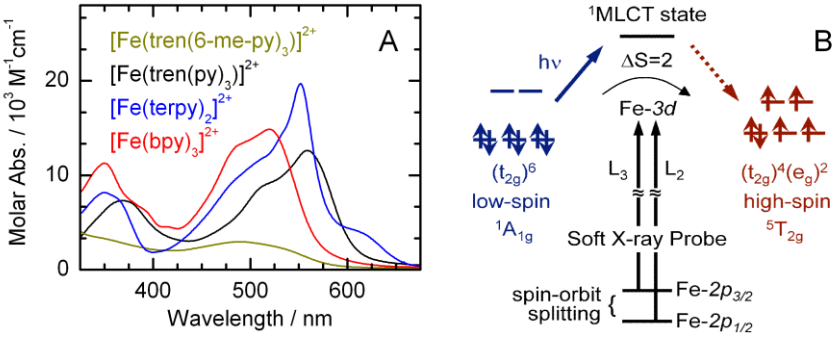

Fig. 3 A Electronic absorption spectra of polypyridyl Fe^{II} compounds in acetonitrile solution. **B** Simplified orbital diagram for an Fe^{II} compound in O_h symmetry, illustrating the probing of the low-spin ground state and the transient high-spin excited state via Fe *2p*→*3d* dipole-allowed core-level transition.

The photo-excited vs. the chemically stabilized high-spin state. Unlike compound **1** which has a low-spin $^1A_1$ ground state at all temperatures, an analogue in which the protons at the 6-positions of the pyridine rings are replaced with methyl groups exhibits a thermal low-spin to high-spin transition at ~210 K.[31,32] For this reason, $[Fe^{II}(6\text{-Me-py})_3tren](PF_6)_2$ has served as a room-temperature high-spin analogue (HSA) in previous studies, allowing for a facile comparison of the HSA ground-state structure and properties with those of the transient high-spin state of the photo-excited compound **1**. Previous results from time-resolved visible and EXAFS spectroscopies at the Fe K-edge,[2,17] clearly illustrated that the structure of the photoexcited high-spin state is very similar to the ground state of $[Fe(tren(6\text{-Me-py})_3)]^{2+}$, thereby validating its use as a proxy for the transiently formed $^5T_2$ state of the photoexcited low-spin species. The recent *ab initio* study by van Kuiken and Khalil[30] also reported substantial structural and electronic resemblance between the transient and chemically stabilized high-spin states. In the following we present experimental results from steady-state and transient x-ray absorption spectroscopy measurements at the Fe $L_{2,3}$-edge which complement and extend the information from previous experimental and *ab initio* results.

Steady-state x-ray absorption spectra of the two solvated compounds at the Fe $L_{2,3}$-edges are displayed in Fig. 4A. Shifts to lower energy and distinct spectral reshaping can be observed for the high-spin analogue as compared to the low-spin $L_{2,3}$-edges of compound **1**. The HSA L_3-peak is 1.8 eV lower in energy than the LS L_3-peak and significantly broader while the centre of the HSA L_2-peak is shifted to lower energy by <1 eV with substantially less intensity than the LS L_2-peak. Great care was taken in the energy calibration of the beamline monochromator to ensure a precision of 0.1 eV during consecutive measurements of the LS and HSA spectra.

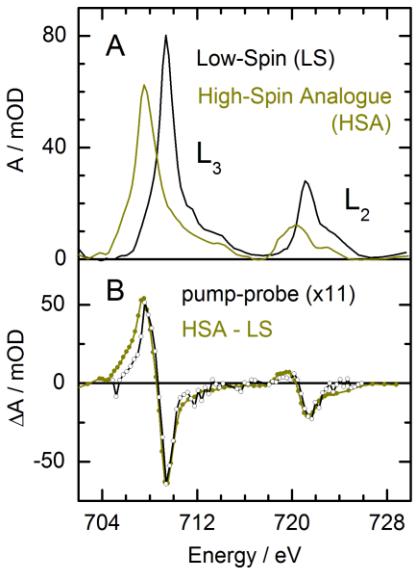

Fig. 4 A Steady-state L-edge spectra of low-spin (LS) $[Fe(tren(py)_3)]^{2+}$ and its high-spin analogue (HSA), both in acetonitrile solution. **B** Difference spectrum (mustard-coloured), HSA-LS, of the steady-state L-edge spectra in panel A and transient difference spectrum (black line) of the photo-excited high-spin and the ground-state low-spin spectrum recorded 150 ps after 400 nm femtosecond pulse excitation of the sample.

Next, we compare the steady-state difference spectrum derived from the data in Fig. 4A with the pump-probe spectrum in Fig. 4B. The rescaling factor of the pump-probe spectrum reflects the fraction of excited molecules x_{exc} = 1/11 which matches well with our estimates based on 400 nm excitation fluence and the molar extinction coefficient. The similarity of the two difference spectra is quite striking. All features are reproduced within the signal-to-noise ratio. The most pronounced difference exists at the L_3-edge. A larger absorption increase of the dispersive HSA-LS spectrum below 707.6 eV indicates that the red-shift of the HSA L_3-edge from that of the LS spectrum is slightly larger than the red-shift of the transient HS L_3-edge. We note that this observation is independent of the uncertainties in the relative absorption of LS and HSA spectra (due to variations in sample concentration and sample thickness) as varying the magnitude of the HSA absorption within experimentally reasonable boundaries shows. Only the maximum absorption loss and gain are affected not their energetic position.

To understand these spectra we will briefly review our previous work:[21] We concluded from comparison of the L_2 and L_3 absorption line shapes with model systems and multiplet calculations that in the low-spin $^1A_1$ ground state, strong π-back-bonding results in delocalization of the Fe *3d*(t_{2g}) electron into the π*-orbitals of the $tren(py)_3$ ligands. The high-spin $^5T_2$ excited state is characterized by suppressed π-back-bonding and attenuated σ-donation from the $tren(py)_3$ ligand relative to the low-spin ground state. Both effects lead to more localized N-*2p* and Fe-*3d* orbitals while keeping the integrated occupancy of the metal-based e_g and t_{2g} orbitals roughly constant, that is, the overall Fe-*3d* charge density is unchanged while the character of the metal-ligand bonding becomes more ionic in nature. These findings agree very well with the *ab initio* study of the Khalil group. From the similarity of the difference spectra in Fig. 4B it is apparent that the HSA ground state is very similar to the transient HS state of compound **1**.

The slightly larger red shift of the high-spin analogue's L_3 peak by ~0.1 eV is a manifestation of the reported small differences in structure[17] and calculated valence charge density[30] between the transient HS state and the steady-state HSA ground state; the latter exhibits slightly larger bond distances and increased structural distortion compared to octahedral symmetry. Origins of the red shift of the transient HS spectrum are the reduction in energy splitting of the Fe t_{2g} and e_g orbitals with increasing bond lengths and increased charge localization.[21] Hence, the spectral difference in Fig. 4B is experimental evidence of the predicted electronic structure of the HSA.

The L_2-edges of transient HS and HSA are essentially identical. The larger absorption increase at the HSA L_3-peak signals a redistribution of absorption from the L_2 to L_3-edge which is commonly a sign of a higher spin-state or a spin admixture but the spin-state has been reported as pure. We think that this behaviour is also a result of the larger deviation from octahedral symmetry of the HSA ground state structure compared to the transient HS state as predicted by van Kuiken and Khalil. We will discuss changes in the relative L_2 and L_3intensity in the context of ligand variations in the next section. Overall, we find great similarity between the

Fe $L_{2,3}$-edges of the transient HS state and the HSA ground state with small spectral disparities attributable to subtle structural differences.

Effects of octahedral distortion. The ligand field in which a transition metal ion is placed has a profound influence on virtually all of the physical properties of the molecule that relate to electronic structure including geometry, optical and magnetic properties, and chemical reactivity. In this context, the question arises what effects ligand variation has on the transient HS state in polypyridyl Fe^{II} complexes and if metal L-edge spectroscopy can detect meaningful differences between the different compounds; the three Fe^{II} polypyridyl complexes we are examining provide a convenient platform on which to begin examining these issues given their similar, but nevertheless distinct, symmetry and compositional characteristics.

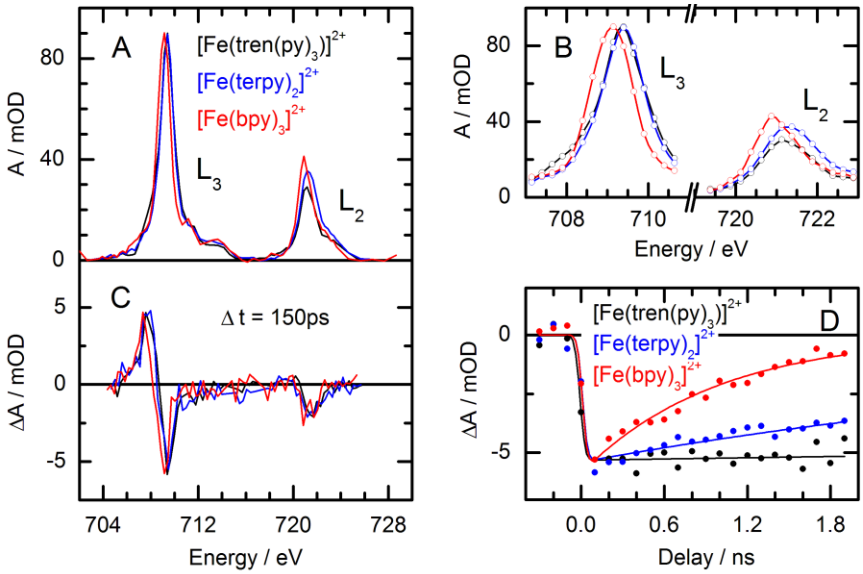

Fig. 5 Comparison of $[Fe(tren(py)_3)]^{2+}$, $[Fe(terpy)_2]^{2+}$, and $[Fe(bpy)_3]^{2+}$ in 100 mM acetonitrile solution **A** steady-state x-ray absorption spectra at the Fe $L_{2,3}$-edges. **B** Spectral zoom of the absorption peaks at the Fe $L_{2,3}$-edges (colour coding as in panel A) **C** Corresponding transient differential x-ray absorption spectra at 150 ps pump-probe delay after excitation with 400 nm light. **D** Pump-probe delay scans at 709.4 eV (dots) and fits to a mono-exponential decay model with decay times as in the published literature (see also text).

Ground state spectra of the three Fe^{II} complexes are shown in Fig. 5A. Absolute absorption differences are not identical due to variation in solubility and sample thickness on the sub-micron scale; after correcting for sample concentration the peak absorption exhibited variances of only ~10%. Accordingly, the ground-state absorption spectra in Fig. 5 have been normalized to the L_3-peak of $[Fe(tren(py)_3)]^{2+}$at 709.4 eV for comparative purposes (black line). The overall spectral shapes are very similar. Compound **1** displays a more distinct shoulder on the low-energy side of the L_3-lineshape (Fig. 5B) which is weaker in compounds **2** and **3**. Given that compound **1** is distinct in possessing two different types of nitrogen donors (pyridine- and imine-based), we believe that this difference is a direct reflection of this compositional variation. Conversely, compound **3** displays the narrowest absorption features which we attribute to the fact that only identical nitrogen donors are present in the $(bpy)_3$ ligand cage, i.e. the highest degeneracy of states exist, while $(terpy)_2$ ligand of compound **2** formally has two types of pyridine nitrogen species. Compounds **1** and **2** show identical peak positions within the spectral precision of ~0.1 eV. In contrast, compound **3** is significantly shifted to lower energy by ~0.2 eV which points to a smaller energy gap between the highest occupied molecular orbital (HOMO) and the lowest unoccupied molecular orbital (LUMO) of $[Fe(bpy)_3]^{2+}$. This is somewhat surprising as one would expect that the ligand systems of compounds **1** and **2** with only pyridine groups have very similar spectral positions.

The branching ratio of the integral $L_{2,3}$-intensities due to Fe *2p→3d* transitions as defined by Thole and co-workers,[33] $r_3 = I(L_3)/[I(L_2)+I(L_3)]$, reports on the spin-state, electrostatic interactions between the core-hole and the valence charge density, and the spin-orbit (SO) interactions between the core-hole and the metal-*3d* manifold as well as within the latter.[33] To properly account for the bound-bound core-level transitions, we have subtracted the continuum edges which are modelled by two arctangents at the $L_{2,3}$-edges with a lifetime broadening of 0.4 eV and 0.2 eV, respectively. Some residual absorption at around 713 eV stems from a Gaussian-like feature in the EXAFS spectrum of the PF_6^- fluorine K-edge. It accounts for 8% of the L_3-edge

intensity and we have corrected the branching ratio accordingly. The branching ratio r_3 equals 0.67 for both the pyridine compounds **2** and **3** with $(terpy)_2$ and $(bpy)_3$ ligands, respectively, while it amounts to 0.71 in compound **1** containing the $tren(py)_3$ ligand. The electronic configuration of the ground state for all three investigated compounds is clearly a singlet state according to Mössbauer spectroscopy.[34] However, for such ground-states the branching ratio is typically ~0.6 while in the absence of electrostatic and SO interactions, the branching ratio is statistical, amounting to $^2/_3$. We conclude from empirical charge-transfer multiplet calculations (see supplementary material for details) that the chemical differences in the ligand cage between compound **1** on one hand and compounds **2** and **3** on the other lead to variations in electrostatic and SO interactions that manifests to a measurable extent in the branching ratio of the ground-state Fe-*2p* spectra as observed in Fig. 5A,B. *Ab initio* multiplet calculations would be very beneficial to gain more detailed insight into the two interactions discussed. While currently no such program code exists, recent developments may soon provide *ab initio* descriptions of third-row transition metal *2p* spectra.[35]

Fig. 5C shows the normalized changes upon 400 nm excitation at a time delay of 150 ps. The spectral features are identical within the signal-to-noise ratio (~0.5 mOD r.m.s.) of the experiment. Identical transient differential spectra mean that the geometric ligand variations among the three samples transmit to the high-spin state in which distortion should increase rather than decrease due to larger bond lengths (the spatial separation of the ligand nitrogen atoms surrounding the metal centre is too short to allow for octahedral symmetry for ground state bond lengths in the first place).

Fig. 5D shows pump-probe delay scans at a fixed probe energy of 709.4 eV, the region of maximal ground state bleaching. These transients are probing ground-state recovery dynamics, i.e., the $^5T_2 \rightarrow {}^1A_1$ relaxation process subsequent to photo-induced formation of the transient high-spin state. The differences in lifetimes inferred from these data are readily understandable within the context of non-radiative decay theory and known variations in high-spin/low-spin zero-point energies across this series; it has been discussed at length in the literature (see Hauser et al.[36] and references therein) and will not be explored further here. We briefly list the published room-temperature $^5T_2$ lifetimes of the three compounds in acetonitrile solution. **1**: τ_{HS} = 60±5 ns, **2**: τ_{HS} = 5.4±0.1 ns, and **3**: τ_{HS} = 980±50 ps. The data in Fig. 5D are wholly consistent with the corresponding optical data over this temporal range, indicating that these x-ray measurements are reliable probes of ground-state recovery, as well (albeit one cannot extract reliable time constants from these particular traces).

Chemical signatures of nearest-neighbour nitrogen atoms. An additional approach to more detailed information concerning metal-ligand interactions in coordination compounds is to focus on the atoms bound to the metal centre(s). These lighter element such as carbon, nitrogen, and oxygen can reveal the 'ligand perspective' by probing their 1s→2π* and higher energy core-level transitions. The former transition probes the LUMO of the metal centre's nearest neighbours while core-level excitation at higher energy reveal spectrally broader continuum resonances which can also be sensitive to the chemical environment and changes thereof.[37] In the following we present data on crystalline films of PF_6-salts of the three compounds in Fig. 1 that we recorded at the Advanced Light Source' EUV calibration beamline 6.3.2 to explore the potential of nitrogen K-edge spectroscopy to elucidate the local chemical environment.

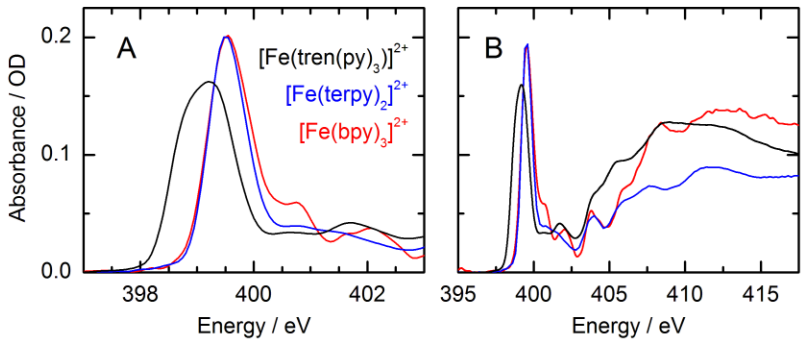

Fig. 6 Ground-state nitrogen K-edge spectra of thin solid films of the complexes in Fig. 1: $[Fe(tren(py)_3)](PF_6)_2$, $[Fe(terpy)_2](PF_6)_2$, and $[Fe(bpy)_3](PF_6)_2$. **A** N 1s→2π* transitions. **B** Wider energy range with N 1s→2π* and σ* shape resonances.

Fig. 6 shows the nitrogen K-edge absorption spectra of compounds **1**, **2**, and **3** around 400 eV. The left panel A features the 1s→2π*. The bipyridine and terpyridine ligands have identical 1s→2π* transitions at 399.5 eV with additional absorption structure characteristic of each ligand. While these two ligand type feature only pyridine ligands, the $tren(py)_3$ ligand cage contains two types of nearest-neighbour nitrogen atoms (those from

the pyridine and the imine groups) which lead to two unresolved transitions centred at 399.2 eV, resulting in a seemingly broader lineshape that reflects the two chemically distinct nitrogen species. These observations are commensurate with the observations of differing branching ratios of compound **1** versus the purely pyridine-based compounds **2** and **3**. However, the latter two compounds show distinct differences in the N K-edge spectra above 400 eV which makes this type of XANES spectroscopy an interesting and chemically specific target.

The same spectra are plotted in Fig. 6B over a wider energy range. In all three spectra a broader absorption feature that starts to rise at 403 eV at energies above the core level ionization threshold as a continuum resonance can be found. The latter may be interpreted as shape resonances, i.e. they can be thought of as unoccupied molecular orbitals embedded in the continuum to which the core-excited electron is promoted. However, there is still some dispute over the nature of these absorption features.[38] Generally, transient nitrogen K-edge edge spectroscopy could prove useful in clarifying whether these resonances provide the so-called 'bond lengths with a ruler' by shifting to higher energy with decreasing chemical bonds. More specifically, this type of spectroscopy on solvated transition-metal complexes could prove very useful in understanding additional details of the metal-ligand interactions. For instance, to address the question of why these complexes, when excited to the MLCT manifold relax to the high-spin $^5T_2$ state with time-constants of ~100 fs without a clear signature of involving metal-centred ligand-field states that are energetically intermediate between the MLCT manifold and the high-spin $^5T_2$ state. One advantage of K-edge spectroscopy in general has been that the core-excited electron can be treated in a one-electron picture which allows for *ab initio* methods to simulate core-level spectra (in contrast to L-edge spectra of first-row transition metals in which multiplets due to strong spin-orbit interactions have complicated the development of *ab initio* methods for core-level spectroscopy). *Ab initio* studies of *1s* transitions of light elements would provide direct comparison with experiment and make details of the valence charge density of the nearest neighbours atoms in transition-metal complexes accessible. Last we note that rapid progress in laser-based high-harmonic sources has led to laser technology with photon energies in the soft x-ray regime.[39] It can be anticipated that in the next years laser-based ultrashort x-ray sources (<30 fs) with sufficient flux at absorption edges in the lower soft x-ray range will allow for femtosecond and possibly attosecond spectroscopy in solution to study charge migration and atomic rearrangement on their natural time scales.

Conclusions

We have studied polypyridyl Fe^{II} complexes in solution with emphasis on the effects of ligand variation on the valence charge density using time-resolved core-level spectroscopy at the Fe $L_{2,3}$-edges. In particular, the transiently excited high-spin state of $[Fe(tren(py)_3)]^{2+}$ and its high-spin analogue have very similar Fe-*2p* spectra which points to the great similarity of the respective valence charge density, complementing previous experimental findings[2,17] and supporting detailed predictions from recent *ab initio* calculations.[30] We further conclude from comparing ground-state and transient iron L-edge spectra of three similar polypyridyl Fe^{II} complexes that the metal valence charge density in these compounds is very similar. However, varying ligand chemical composition and possibly structural differences alter electrostatic and spin-orbit interactions which in turn could be an important factor influencing the high-spin relaxation rate. Additionally, ultrafast spectroscopy at the K-edges of the nearest-neighbours of metal centres in solvated transition-metal compounds is proposed to probe the 'ligand view' of the metal-ligand interactions. Such measurements will provide complementary information on the valences charge density of short-lived intermediates in combination with newly developed *ab initio* methods for core-level spectroscopy. We anticipate that advances in laser technology will allow for 'table-top' experiments in the foreseeable future with time-resolution approaching the fundamental time-scales of charge transfer. Such techniques could shed further light on elementary chemical processes beyond the prototypical iron complexes studied in this work.

Acknowledgements

This work was supported by the Director, Office of Science, Office of Basic Energy Sciences, the Chemical Sciences, Geosciences, and Biosciences Division under the Department of Energy, Contract No. DE-AC02-05CH11231 (N.H., H.C., and R.W.S.) and Grant No. DE-FG02-01ER15282 (J.K.M.), as well as the National Research Foundation of Korea (NRF) grants funded by the Korea government (MEST) (No. 2009-0068446, 2010-0006570, and 2007-0056330) (H. C., K. H., and T.K.K.).

References

1 S. Ferrere and B. A. Gregg, *J. Am. Chem. Soc.*, 1998, **120**, 843.
2 J. E. Monat and J. K. McCusker, *J. Am. Chem. Soc.*, 2000, **122**, 4092.
3 C. Creutz, M. Chou, T. L. Netzel, M. Okumura and N. Sutin, *J. Am. Chem. Soc.*, 1980, **102**, 1309.
4 J. J. McGravey and I. Lawthers, *J. Chem. Soc., Chem. Commun.*, 1982, 902.
5 E. Buhks, G. Navon, M. Bixon and J. Jortner, *J. Am. Chem. Soc.*, 1980, **102**, 2918.
6 S. Decurtins, P. Gütlich, C. Köhler, H. Spiering and A. Hauser, *Chem. Phys. Lett.*, 1984, **105**, 1.
7 C. L. Xie and D. N. Hendrickson, *J. Am. Chem. Soc.*, 1987, **109**, 6981.
8 P. Gütlich and A. Hauser, *Coord. Chem. Rev.*, 1990, **97**, 1.
9 A. Hauser, A. Vef and P. Adler, *J. Chem. Phys.*, 1991, **95**, 8710.
10 J. K. McCusker, K. N. Walda, R. C. Dunn, J. D. Simon, D. Magde and D. N. Hendrickson, *J. Am. Chem. Soc.*, 1992, **114**, 6919.
11 J. K. McCusker, K. N. Walda, R. C. Dunn, J. D. Simon, D. Magde and D. N. Hendrickson, *J. Am. Chem. Soc.*, 1993, **115**, 298.
12 A. L. Smeigh, M. Creelman, R. A. Mathies and J. K. McCusker, *J. Am. Chem. Soc.*, 2008, **130**, 14105.
13 W. Gawelda, A. Cannizzo, V.-T. Pham, F. van Mourik, C. Bressler and M. Chergui, *J. Am. Chem. Soc.*, 2007, **129**, 8199.
14 C. de Graaf and C. Sousa, *Chem. Eur. J.*, 2010, **16**, 4550.
15 M. M. N. Wolf, R. Groß, C. Schumann, J. A. Wolny, V. Schünemann, A. D, H. Paulsen, J. J. McGarvey and R. Diller, *Phys. Chem. Chem. Phys.*, 2008, **10**, 4264.
16 C. Consani, M. Prémont-Schwarz, A. ElNahhas, C. Bressler, F. van Mourik, A. Cannizzo and M. Chergui, *Angew. Chem. Int. Ed.*, 2009, **48**, 7184.
17 M. Khalil, M. A. Marcus, A. L. Smeigh, J. K. McCusker, H. H. W. Chong and R. W. Schoenlein, *J. Phys. Chem. A*, 2006, **110**, 38.
18 W. Gawelda, V.-T. Pham, M. Benfatto, Y. Zaushitsyn, M. Kaiser, D. Grolimund, S. L. Johnson, R. Abela, A. Hauser, C. Bressler and M. Chergui, *Phys. Rev. Lett.*, 2007, **98**, 057401.
19 C. Bressler, C. Milne, V.-T. Pham, A. ElNahhas, R. M. van der Veen, W. Gawelda, S. Johnson, P. Beaud, D. Grolimund, M. Kaiser, C. N. Borca, G. Ingold, R. Abela and M. Chergui, *Science*, 2009, **323**, 489.
20 S. Nozawa, T. Sato, M. Chollet, K. Ichiyanagi, A. Tomita, H. Fujii, S.-i. Adachi and S.-y. Koshihara, *J. Am. Chem. Soc.*, 2010, **132**, 61.
21 N. Huse, T. K. Kim, L. Jamula, J. K. McCusker, F. M. de Groot and R. W. Schoenlein, *J. Am. Chem. Soc.*, 2010, **132**, 6809.
22 G. Vankó, P. Glatzel, V.-T. Pham, R. Abela, D. Grolimund, C. N. Borca, S. L. Johnson, C. J. Milne and C. Bressler, *Angew. Chem. Int. Ed.*, 2010, **49**, 1.
23 N. Huse, H. Cho, K. Hong, L. Jamula, F. M. de Groot, T. K. Kim, J. K. McCusker and R. W. Schoenlein, *J. Phys. Chem. Lett.*, 2011, **2**, 880.
24 L. X. Chen, W. J. H. Jager, G. Jennings, D. J. Gosztola, A. Munkholm and J. P. Hessler, *Science*, 2001, **292**, 262.
25 C. Bressler and M. Chergui, *Chem. Rev.*, 2004, **104**, 1781.
26 P. Wernet, G. Gavrila, K. Godehusen, C. Weniger, E. Nibbering, T. Elsaesser and W. Eberhardt, *Appl. Phys. A: Mater. Sci. Process.*, 2008, **92**, 511.
27 N. Huse, H. Wen, D. Nordlund, E. Szilagyi, D. Daranciang, T. A. Miller, A. Nilsson, R. W. Schoenlein and A. M. Lindenberg, *Phys. Chem. Chem. Phys.*, 2009, **11**, 3951.
28 N. Huse, H. Wen, R. W. Schoenlein and A. M. Lindenberg, *J. Chem. Phys.*, 2009, **131**, 234505.
29 M. Lorenc, J. Hébert, N. Moisan, E. Trzop, M. Servol, M. Buron-Le Cointe, H. Cailleau, M. Boillot, E. Pontecorvo, M. Wulff, S. Koshihara and E. Collet, *Phys. Rev. Lett.*, 2009, **103**, 028301.
30 B. E. Van Kuiken and M. Khalil, *J. Phys. Chem. A*, 2011, **115**, 10749.
31 K. M. Kadish, C. H. Su, D. Schaeper, C. L. Merrill and L. J. Wilson, *Inorg. Chem.*, 1982, **21**, 3433.
32 A. J. Conti, C. L. Xie and D. N. Hendrickson, *J. Am. Chem. Soc.*, 1989, **111**, 1171.
33 B. T. Thole and G. van der Laan, *Phys. Rev. B*, 1988, **38**, 3158.
34 V. Briois, C. C. dit Moulin, P. Sainctavit, C. Brouder and A.-M. Flank, *J. Am. Chem. Soc.*, 1995, **117**, 1019.
35 P. Wernet, private communication.
36 A. Hauser, C. Enachescu, M. L. Daku, A. Vargas and N. Amstutz, *Coord. Chem. Rev.*, 2006, **250**, 1642.
37 J. M. Garcia-Lastra, P. L. Cook, F. J. Himpsel and A. Rubio, *J. Chem. Phys.*, 2010, **133**, 151103.
38 M. Piancastelli, *J. Electron. Spectrosc. Relat. Phenom.*, 1999, **100**, 167.
39 M.-C. Chen, P. Arpin, T. Popmintchev, M. Gerrity, B. Zhang, M. Seaberg, D. Popmintchev, M. M. Murnane and H. C. Kapteyn, *Phys. Rev. Lett.*, 2010, **105**, 173901.

DISCLAIMER